Chinese Chemical Letters 34 (2023) 107542

Contents lists available at ScienceDirect

Chinese Chemical Letters

journal homepage: www.elsevier.com/locate/cclet

Self-enhanced photothermal-chemodynamic antibacterial agents for synergistic anti-infective therapy

Ning Guo[a], Yu Xia[a], Yuxi Duan[a], Quanxin Wu[a], Le Xiao[a], Yaxin Shi[a], Bin Yang[b,*], Yun Liu[a,c,*]

[a] Guangdong Key Laboratory for Research and Development of Natural Drugs, School of Pharmacy, Guangdong Medical University, Zhanjiang 524023, China
[b] The Sixth Affiliated Hospital of Guangzhou Medical University, Qingyuan People's Hospital; Department of Biomedical Engineering, School of Basic Medical Sciences, Guangzhou Medical University, Guangzhou 511436, China
[c] The Marine Biomedical Research Institute of Guangdong, Zhanjiang 524023, China

ARTICLE INFO

Article history:
Received 27 January 2022
Revised 13 May 2022
Accepted 17 May 2022
Available online 21 May 2022

Keywords:
Antibacterial
Self-enhanced
Photothermal therapy
Chemodynamic therapy
Anti-infective therapy

ABSTRACT

$Cu_{2-x}S$ nanostructures have been intensively studied as outstanding chemodynamic therapy (CDT) and good photothermal therapy (PTT) antibacterial agents due to their highly efficient Cu(I)-initiated Fenton-like catalytic activity and good photothermal conversion property. However, they still suffer from shortage of Cu(I) supply in the long-term and comparatively low inherent photothermal conversion efficiency. Herein, we constructed a self-enhanced synergistic PTT/CDT nanoplatform ($Cu_{1.94}S$@MPN) by coating $Cu_{1.94}S$ nanoparticles with Fe(III)/tannic acid based metal-polyphenol networks (MPN). Activated by the acidic bacterial infection microenvironment, $Cu_{1.94}S$@MPN could be decomposed to continuously release Cu(II), Fe(III) ions and tannic acid. As the result of tannic acid-involved Cu and Fe redox cycling, Cu(I)/Fe(II)-rich CDT could be achieved through the highly accelerated catalytic Fenton/Fenton-like reactions. More importantly, experimental results demonstrated that $Cu_{1.94}S$@MPN exhibited both excellent photothermal antibacterial and photothermal-enhanced CDT properties to eradicate bacteria *in vitro* and *in vivo*. Overall, this novel nanotherapeutics has great potential to become a clinic candidate for anti-infective therapy in future.

In the past few years, intensive research efforts have been devoted to bacterial infection due to the high infection probability and serious mortality, particularly in the context of infectious diseases spread [1–7]. In clinical trials, the utilization of antibiotics is often the first choice for anti-infective therapy. However, long-term use and abuse of antibiotics (such as excess, insufficiency and defective use) have led to the occurrence of antimicrobial resistance (AMR) [8–10]. Unfortunately, the discovery of novel types of antibiotics has significantly lagged behind the rapid spread of AMR [11]. In 2014, the World Health Organization (WHO) predicted that the issue of AMR could cause the death of nearly 10 million people each year by 2050 in a published review [12]. Therefore, the development of novel non-antibiotic therapies for bacterial infection, which could prevent the occurrence of AMR, is becoming increasingly significant.

Recently, promising approaches with negligible AMR have been proposed for anti-infective treatments [13–17], for instance, chemodynamic therapy (CDT) [18–20] and photothermal therapy (PTT) [21–26]. CDT takes full advantage of Fe(II)-initiated Fenton reaction or Cu(I)-initiated Fenton-like reaction to kill bacteria [27]. During the process, endogenous hydrogen peroxide (H_2O_2) at the infection site is efficiently degraded to produce highly destructive hydroxyl radicals ($^{\bullet}OH$) for effective bacterial inactivation. Besides, it is worth to mention that CDT greatly benefits from acidity and overexpressed H_2O_2 level in the infected tissue [28,29]. Meanwhile, increasing research attention has also been focused on PTT due to its broad-spectrum antibacterial capacity and excellent controllability *via* near-infrared (NIR) light. To further improve the therapeutic efficiency and minimize adverse effects, the strategy of combining PTT with CDT has been reported recently [30]. More importantly, synergistic PTT/CDT not only can directly kill bacteria *via* PTT or CDT themselves, but also leads to the self-enhanced therapeutic efficacy of CDT through increasing the local temperature with PTT [31–34]. Hence, PTT/CDT synergistic therapeutic nanoagents could be promising candidates in clinical trials.

* Corresponding authors.
E-mail addresses: bin.yang@gzhmu.edu.cn (B. Yang), liuyun_2017@hotmail.com (Y. Liu).

https://doi.org/10.1016/j.cclet.2022.05.056
1001-8417/

In this regard, $Cu_{2-x}S$ nanostructures with variable oxidation states (I/II), possessing good photothermal conversion property in the NIR region and efficient Fenton-like catalytic activity, have been exploited as PTT and highly efficient CDT therapeutic agents for anti-infective therapy [35–37]. It was reported that Cu(I)-initiated Fenton-like reaction is featured with dramatically higher reaction rate ($\approx 1 \times 10^4$ L mol^{-1} s^{-1}) than that of Fe(II)-initiated Fenton reaction (≈ 63 L mol^{-1} s^{-1}) [38]. However, their antibacterial applications are still limited due to their comparatively low photothermal conversion efficiency ($\eta \approx 25.7\%$). On the other hand, metal-polyphenol networks (MPN) formed by Fe(III) and tannic acid (TA, Scheme S1 in Supporting information) or other polyphenols have been also used as CDT and PTT agents for both cancer and anti-infective therapies [39–42]. In the presence of solid templates, MPN-based nano-coatings could be formed onto the interface of templates. Despite the continuous Fe(II) ions supply through reducing Fe(III) with TA, Fe(III)/TA based MPN still suffer from unsatisfactory CDT efficacy due to the inherent low reaction rate of Fe(II)-initiated Fenton reaction. Interestingly, compared with $Cu_{2-x}S$ nanostructures ($\eta \approx 25.7\%$), Feng and coworkers reported that Fe(III)/TA based MPN illustrated more excellent photothermal conversion property ($\eta \approx 45.4\%$) for PTT [43].

Based on the above mentioned, we designed a novel self-enhanced PTT/CDT antibacterial nanoagent by engineering $Cu_{1.94}S$ nanoparticles with Fe(III)/TA based MPN nano-coatings, named $Cu_{1.94}S$@MPN, to achieve non-antibiotic synergistic anti-infective therapy. As illustrated in Scheme 1, $Cu_{1.94}S$ with good photothermal conversion property and excellent catalytic capacity were prepared *via* a simple and low-cost published protocol [44]. Further modification of $Cu_{1.94}S$ with Fe(III)/TA based MPN could not only improve their biocompatibility, but also achieve self-enhanced PTT/CDT synergistic therapeutic effect. After *in situ* injection, interior $Cu_{1.94}S$ could serve as both the source of Cu(I) ions for Cu(I)-initiated CDT and photothermal agents for PTT. In this nanotherapeutics, exterior MPN were employed as PTT agents due to their outstanding photothermal property. More importantly, MPN could dissociate with the continuous release of Fe(III) and TA in response to acidic pH in infected tissues. Owning to the reducing function of TA, Fe(III) and Cu(II) could be converted into Fe(II) and Cu(I) with accelerated redox cycling to achieve enhanced CDT. Therefore, a perfect nanotherapeutics, which integrated photothermal eradication and photothermal-enhanced CDT, was successfully constructed by the combination of $Cu_{1.94}S$ with MPN for mutual profit in anti-infective therapy. The current protocol will offer new concepts for developing efficient treatments of bacterial infection in clinic trials.

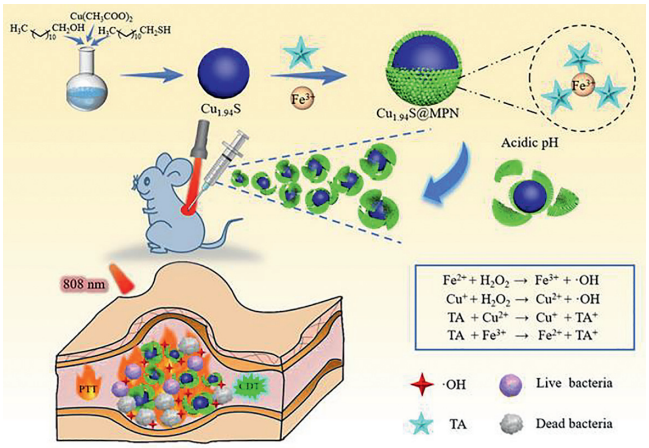

Scheme 1. Schematic representation of the production of $Cu_{1.94}S$@MPN and its synergistic antibacterial therapy.

Detailed synthetic procedures of $Cu_{1.94}S$@MPN were presented in Supporting information. Afterwards, $Cu_{1.94}S$@MPN was fully characterized by transmission electron microscopy (TEM), dynamic light scattering (DLS), X-ray photoelectron spectroscopy (XPS), X-ray diffraction (XRD), Fourier transform infrared (FT-IR) and ultra violet-visible-near infrared (UV-vis-NIR) spectrophotometric analysis (Scheme 1, Figs. 1a-c and Fig. S1 in Supporting information). TEM images showed the spherical nanostructures and nanosizes of $Cu_{1.94}S$ and $Cu_{1.94}S$@MPN (Fig. 1a, Fig. S1a). On the other hand, their hydrodynamic diameters determined by DLS analysis were ~60 nm for $Cu_{1.94}S$ and ~170 nm for $Cu_{1.94}S$@MPN, separately (Fig. 1b and Fig. S1b). Obviously, the size of $Cu_{1.94}S$@MPN was much larger than that of $Cu_{1.94}S$ after modification. Due to the same reason, zeta potential of $Cu_{1.94}S$@MPN became more negative (Fig. 1c). As can be seen from Fig. S1c, $Cu_{1.94}S$@MPN showed two peaks of Cu $2p_{3/2}$ at 932.6 eV and Cu $2p_{1/2}$ at 952.6 eV with no visible satellite peak in the Cu 2p region, which illustrated that the valence state of Cu in $Cu_{1.94}S$@MPN was mainly +1 [45]. In addition, the crystalline structure of $Cu_{1.94}S$ in $Cu_{1.94}S$@MPN was recorded by XRD analysis. As displayed in Fig. S1d, the characteristic pattern of $Cu_{1.94}S$@MPN was in accordance with $Cu_{1.94}S$ (JCPDS No. 34-0660), which suggested that the crystal structure of $Cu_{1.94}S$ was not affected by MPN layer. Besides, the FT-IR spectrum of $Cu_{1.94}S$@MPN illustrated typical peaks (1400–1600 cm^{-1}) corresponding to benzene rings of TA (Fig. S1e), which further proved the successful synthesis of $Cu_{1.94}S$@MPN. In brief, all these characterizations solidly demonstrated the successful production of $Cu_{1.94}S$@MPN.

Furthermore, the photothermal and peroxidase-like catalytic properties of $Cu_{1.94}S$@MPN were systemically investigated. As can be seen from Fig. S1f, $Cu_{1.94}S$@MPN showed a relatively high absorbance at 808 nm, which indicated its photothermal conversion effect under 808 nm laser activation. Technically, the photothermal performance of $Cu_{1.94}S$@MPN was studied by illuminating $Cu_{1.94}S$@MPN of different concentrations with an 808 nm laser at various power densities (Figs. 1d-f and Fig. S2a in Supporting information). Upon irradiation, the temperature differences were found to be concentration and power density dependent. Meanwhile, its photothermal property exhibited no big decrement after ten cycles, which proved its extraordinary photostability (Fig. 1f). By using single "on-off" laser irradiation assay, its photothermal conversion efficiency (η) was determined to be 29.17% (Figs. S2b and c in Supporting information). These experimental outcomes proved the remarkable photothermal effect of $Cu_{1.94}S$@MPN as an encouraging PTT nanoagent. Due to the typical absorption peak at 652 nm after oxidization, 3,3′,5,5′-tetramethylbenzidine (TMB) was utilized as a probe to verify the formation of ·OH (Figs. 1g and h, Fig. S3 in Supporting information). Similarly, the catalytic activity of $Cu_{1.94}S$@MPN showed concentration and time dependent properties, which was also influenced by the concentration of H_2O_2. Compared with $Cu_{1.94}S$, the peroxidase-like catalytic ability of $Cu_{1.94}S$@MPN was greatly facilitated by MPN, which was attributed to its outstanding photothermal effect and successive Cu(I) ions supply through the pH-responsive degradation of $Cu_{1.94}S$@MPN (Fig. S4 in Supporting information) and the reduction of Cu(II) with TA. Eventually, these results demonstrated that $Cu_{1.94}S$@MPN could be a promising antibacterial nanoagent for self-enhanced synergistic PTT/CDT.

Encouraged by above outcomes, *in vitro* antibacterial and antibiofilm capacities of $Cu_{1.94}S$ and $Cu_{1.94}S$@MPN were assessed by plate counting method against *S. aureus* and *E. coli* at pH 5.5 (Figs. 2 and 3, Figs. S5-S7 in Supporting information). During the assays, bacteria were dealt with $Cu_{1.94}S$ and $Cu_{1.94}S$@MPN under four types of conditions, including NIR(−)H_2O_2(−), NIR(−)H_2O_2(+), NIR(+)H_2O_2(−) and NIR(+)H_2O_2(+). Initially, $Cu_{1.94}S$ showed severely limited antibacterial activity under all conditions even

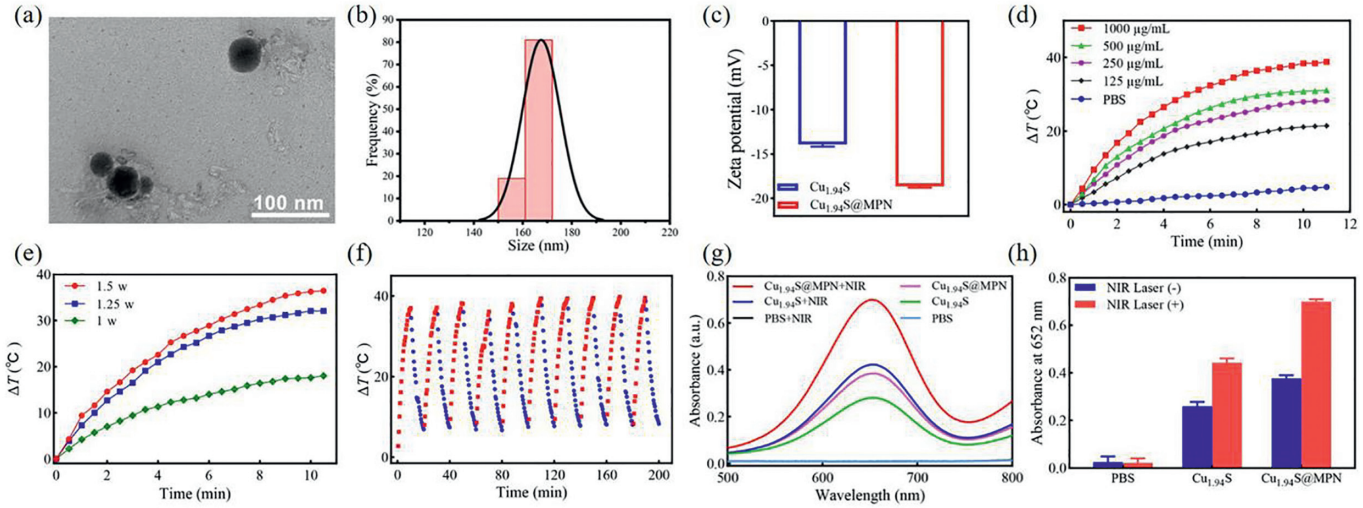

Fig. 1. (a) TEM image of $Cu_{1.94}S$@MPN. (b) Dynamic light scattering spectrum of $Cu_{1.94}S$@MPN. (c) Zeta potential profiles of $Cu_{1.94}S$ and $Cu_{1.94}S$@MPN. Temperature changes of $Cu_{1.94}S$@MPN aqueous solution irradiated by an 808 nm laser (d) at different concentrations (1.25 W/cm^2), (e) at different power densities (500 μg/mL). (f) Heating and cooling curves of $Cu_{1.94}S$@MPN aqueous solution (500 μg/mL) over 10 cycles of irradiation (808 nm, 1.25 W/cm^2). (g) and (h) Absorbance of TMB solutions at 652 nm *via* incubating with $Cu_{1.94}S$ and $Cu_{1.94}S$@MPN at pH 5.5 in the presence H_2O_2.

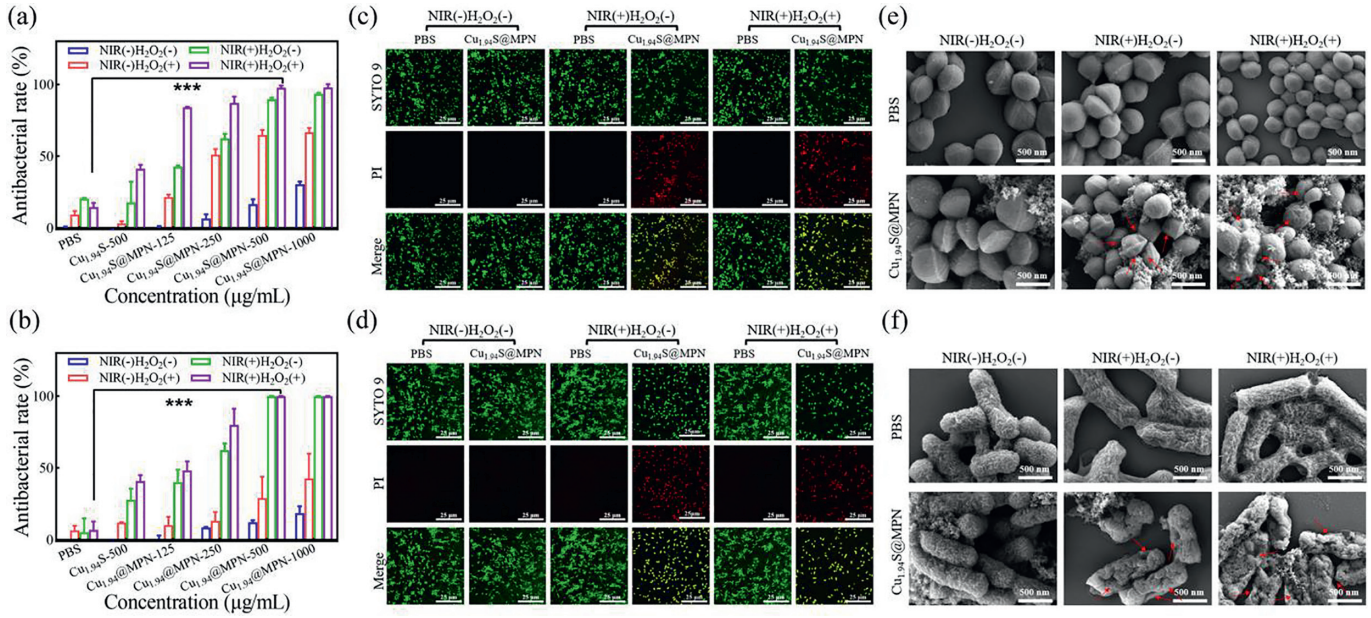

Fig. 2. Antibacterial rate of (a) *S. aureus* and (b) *E. coli* after different treatments determined by the plate counting method. Fluorescence staining images of (c) *S. aureus* and (d) *E. coli*. Dead/live bacteria are labeled green by SYTO 9, and dead bacteria are labeled red by PI (scale bar: 25 μm). SEM images of (e) *S. aureus* and (f) *E. coli* after different treatments (scale bar: 500 nm). $Cu_{1.94}S$@MPN-500 means the concentration of $Cu_{1.94}S$@MPN is 500 μg/mL, NIR(+)H_2O_2(+) means the samples were irradiated by an 808 nm laser light (1.25 W/cm^2) for 10 min in the presence of H_2O_2 (100 μmol/L).

at concentration of 500 μg/mL (Figs. 2a and b, Fig. S5). Likewise, $Cu_{1.94}S$@MPN exhibited badly restricted efficiency under the condition of NIR(−)H_2O_2(−). Upon irradiation (1.25 W/cm^2, NIR(+)H_2O_2(−)), $Cu_{1.94}S$@MPN displayed a concentration depended PTT efficiency and reached ~90% antibacterial activity until 1000 μg/mL. Under the condition of NIR(−)H_2O_2(+), similar outcomes as PTT were obtained, such as concentration dependence of CDT effect and a badly restrained antibacterial activity until 1000 μg/mL. Anyhow, monotherapy could not achieve satisfactory efficiency at a relatively low concentration of $Cu_{1.94}S$@MPN. Upon the usage of an 808 nm laser light, synergistic PTT/CDT was performed with $Cu_{1.94}S$@MPN, and realized greatly enhanced efficiencies of 91.9% (*S. aureus*) and 98.1% (*E. coli*), separately. Live/dead bacterial staining assays were performed by employing SYTO-9 and PI staining kits. Notably, more intensive red fluorescence were viewed in $Cu_{1.94}S$@MPN groups under the condition of NIR(+)H_2O_2(+) compared with other groups (Figs. 2c and d). Meanwhile, the morphological changes of bacteria were observed by scanning electron microscopy (SEM). Compared to other groups, more massive wrinkles and dents were generated in $Cu_{1.94}S$@MPN group under the condition of NIR(+)H_2O_2(+), manifested its outstanding antibacterial ability *via* synergistic PTT/CDT (Figs. 2e and f). Apart from planktonic bacteria, the destructive capacities towards stubborn biofilms were further evaluated under the same conditions by plate counting method (Figs. 3a-d and Fig. S7). At the beginning, uniform biofilms of *S. aureus* and *E. coli* were formed and stained with crystal violet (Fig. S7). Afterwards, synergistic PTT/CDT with $Cu_{1.94}S$@MPN was found to show the highest effi-

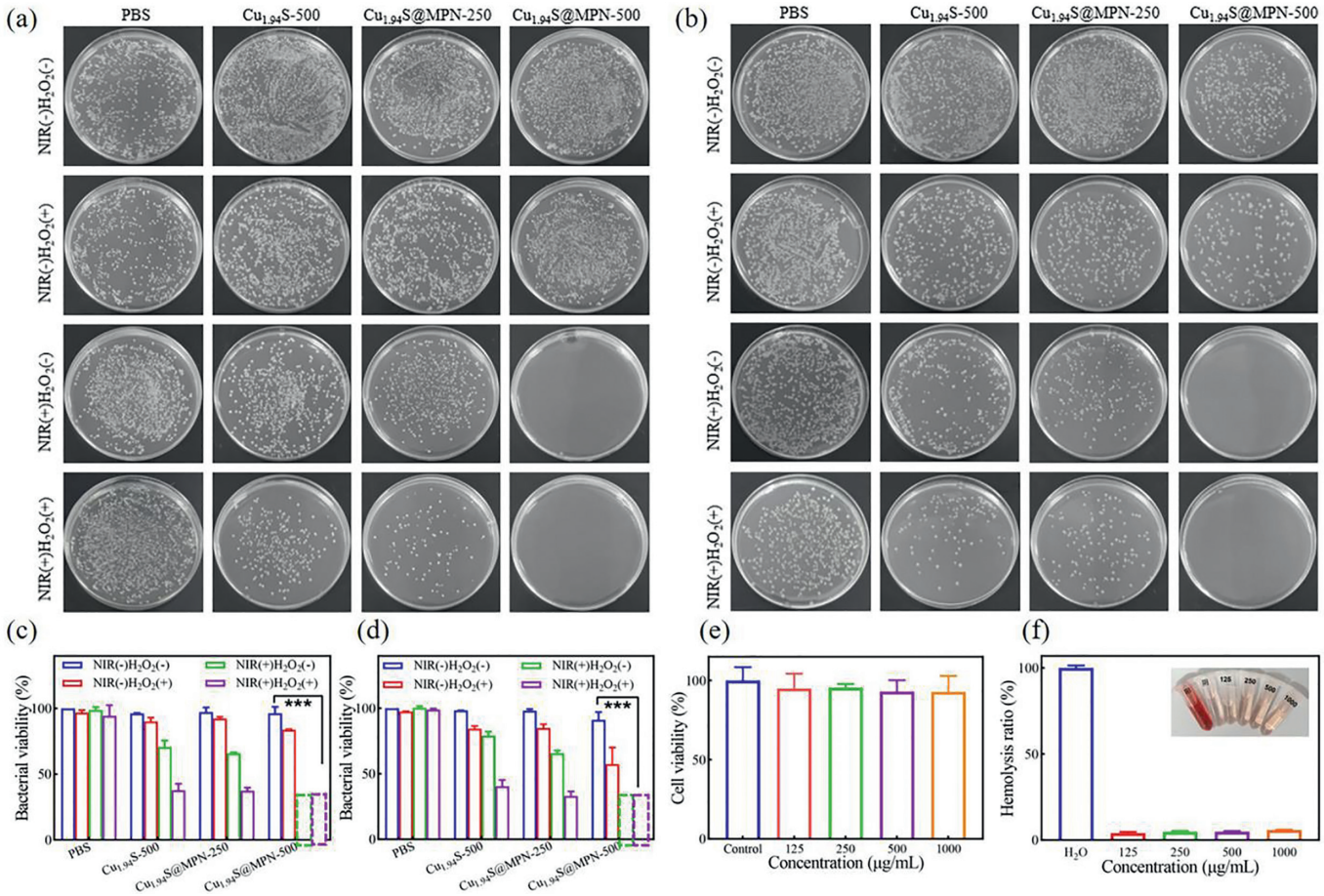

Fig. 3. Representative plate photographs of (a) *S. aureus* and (b) *E. coli* colonies detached from respective biofilms and their corresponding antibiofilm activity against (c) *S. aureus* and (d) *E. coli*. (e) Cell viability of L929 cells treated with different concentrations of $Cu_{1.94}S$@MPN. (f) Relative hemolysis rate of DI water, PBS and different concentrations of $Cu_{1.94}S$@MPN. Insets are the corresponding photographs. $Cu_{1.94}S$@MPN-500 means the concentration of $Cu_{1.94}S$@MPN is 500 μg/mL, NIR(+)H_2O_2(+) means the samples were irradiated by an 808 nm laser light (1.25 W/cm^2) for 10 min in the presence of H_2O_2 (100 μmol/L).

ciency in anti-biofilm assays (Figs. 3a-d) and led to an absolute damage of biofilms (>99%) at 500 μg/mL. Basically, all acquired results implied the outstanding bactericidal ability of $Cu_{1.94}S$@MPN.

Furthermore, MTT and hemolysis assays were used to appraise the biosafety of $Cu_{1.94}S$@MPN (Figs. 3e and f). After incubating with L929 cells, negligible cytotoxicity was observed even at a quite high concentration (1000 μg/mL, Fig. 3e). In the hemolytic test, mouse red blood cells (RBCs) treated with H_2O was employed as positive control and PBS as negative control. Inspiringly, the hemolysis rate of $Cu_{1.94}S$@MPN was merely 5.8% at the concentration of 1000 μg/mL (Fig. 3f). Virtually, the perfect biosafety of $Cu_{1.94}S$@MPN was proved by these results.

Motivated by the perfect antibacterial ability and biocompatibility of $Cu_{1.94}S$@MPN *in vitro*, *S. aureus* infected subcutaneous mice model was utilized to evaluate its *in vivo* therapeutic efficiency in Balb/c mice (Fig. 4, Figs. S8 and S9 in Supporting information) approved by the Ethics Committee of Guangdong Medical University. After infected for 1 day, all mice were randomly divided into four groups, namely, PBS group, PBS+NIR group, $Cu_{1.94}S$@MPN group and $Cu_{1.94}S$@MPN+NIR group. PBS was *in situ* injected into infection site of mice in control groups, while $Cu_{1.94}S$@MPN was administrated in therapeutic groups (Fig. 4a). Meanwhile, NIR irradiation was given to PBS+NIR and $Cu_{1.94}S$@MPN+NIR groups (Fig. S8a). The images of infected tissues and body weight of every mouse were daily recorded during the entire 15-day treatment period (Fig. 4b and Fig. S8b). In PBS, PBS+NIR and $Cu_{1.94}S$@MPN groups, persistent pustules existed until the end of treatment. In contrary, gradually diminished scars were observed in $Cu_{1.94}S$@MPN+NIR group due to synergistic PTT/CDT. After the homogenization treatment of the acquired infected tissues in saline on day 5, the antibacterial ability of $Cu_{1.94}S$@MPN was quantificationally assessed by plate counting method (Figs. 4c and d). Compared with PBS group, the amount of colonies diminished to 38.72% for $Cu_{1.94}S$@MPN group due to the limited CDT effect of $Cu_{1.94}S$@MPN in the absence of NIR. Encouragingly, $Cu_{1.94}S$@MPN+NIR group achieved an antibacterial rate of 84.93%, indicating the excellent *in vivo* bactericidal capacity of $Cu_{1.94}S$@MPN mediated synergistic PTT/CDT. At end of the treatment, the serum of infected mice was collected to evaluate the expression levels of several characteristic pro-inflammatory cyto-kines through enzyme-linked immunosorbent assay (ELISA), including TNF-α, IL-6 and IL-1β (Figs. 4e-g). The levels of all pro-inflammatory cyto-kines after treatment were found to be significantly decreased in comparison with PBS and PBS+NIR groups. Even better, the levels for $Cu_{1.94}S$@MPN+NIR group showed no obvious statistical distinction compared to normal mice, which demonstrated the reduced inflammation through synergistic PTT/CDT. On the other hand, the skin at infected site was also obtained for hematoxylin and eosin (H&E) staining (Fig. 4h). The same as normal tissues, no apparent inflammatory cells were observed in $Cu_{1.94}S$@MPN+NIR group, further verifying its remarkable *in vivo* anti-inflammatory effect.

In summary, a novel infection microenvironment-responsive antibacterial nanoplatform $Cu_{1.94}S$@MPN was constructed by encapsulating $Cu_{1.94}S$ with Fe(III)/TA based MPN nano-shells. Due to

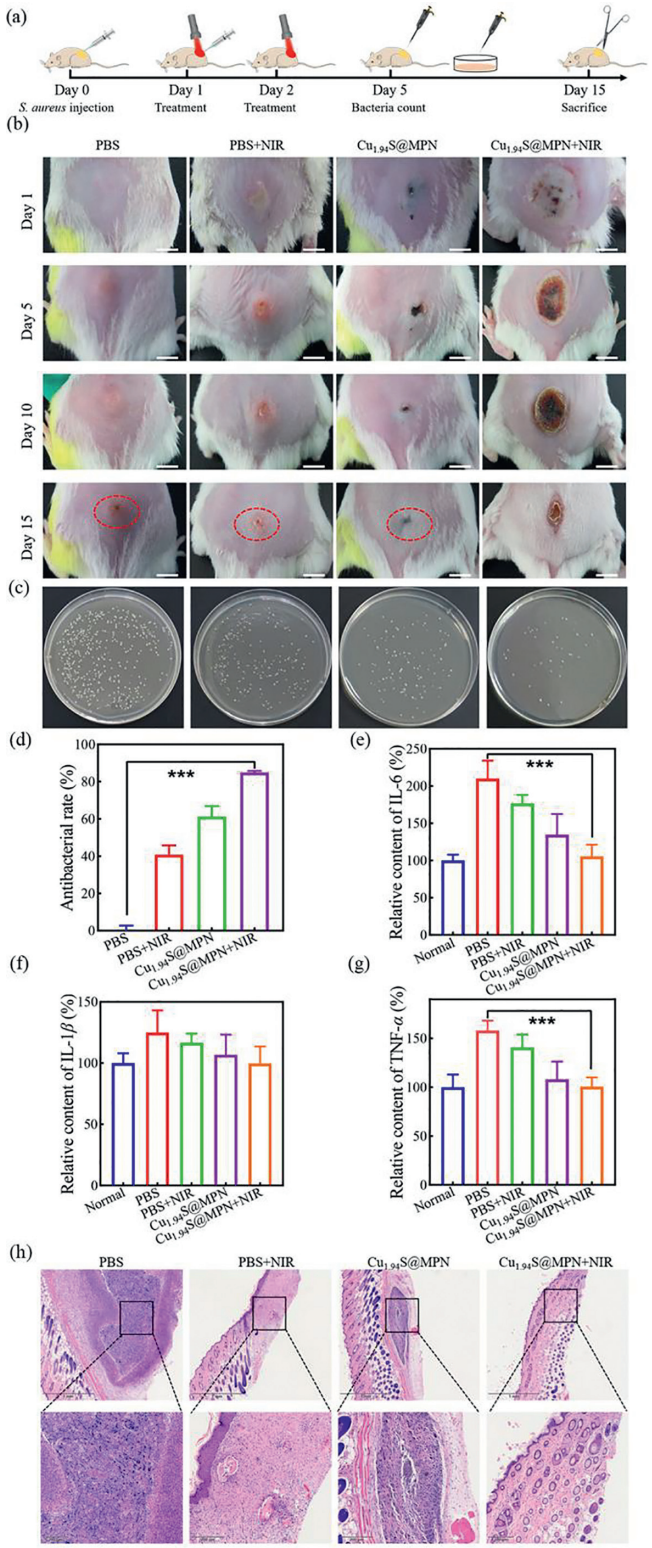

Fig. 4. (a) Schematic illustration of the treatment process of the mouse subcutaneous abscess model. (b) Photographs of infected area on the infected mice treated with PBS, PBS+NIR, $Cu_{1.94}S$@MPN, $Cu_{1.94}S$@MPN+NIR at different time points (scale bar: 5 mm). (c) Representative photographs of bacterial colonies from infected wound area of different treatment groups after 5 days. (d) Antibacterial rate of the infected tissues on day 5 determined by the plate counting method. (e) IL-6, (f) IL-1β and (g) TNF-α levels of infected mice serum tested by ELISA on day 15 (***$P<0.001$). (h) H&E staining images of the infected tissues from the four groups after 15 days (scale bar: 1 mm and 200 μm). NIR(+)H_2O_2(+) means the samples were irradiated by an 808 nm laser light (1.25 W/cm^2) for 10 min in the presence of H_2O_2 (100 μmol/L).

the excellent inherent photothermal conversion property of MPN and continuous Cu(I) ions supply *via* reducing Cu(II) with TA, it achieved self-boosted synergistic PTT/CDT with extraordinary efficiency. Antibacterial experiments proved that $Cu_{1.94}S$@MPN could achieve a satisfactory bactericidal activity both *in vitro* and *in vivo*. This research might offer new strategy on developing intelligent nanotherapeutics for anti-bacterial therapy in clinical trials.

Declaration of competing interest

The authors declare that they have no known competing financial interests or personal relationships that could have appeared to influence the work reported in this paper.

Acknowledgments

This research was financially supported by the National Natural Science Foundation of China (Nos. 81803723, 51903062), Guangdong Basic and Applied Basic Research Foundation (No. 2019B1515120006), Guangdong Province Universities and Colleges Pearl River Scholar Funded Scheme (2019), Innovation and Entrepreneurship Team Leads the Pilot Program of Zhanjiang (No. 2020LHJH005), Discipline Construction Project of Guangdong Medical University (No. 4SG22002G) and Science and Technology Projects of Guangzhou (No. 202102020757).

Supplementary materials

Supplementary material associated with this article can be found, in the online version, at doi:10.1016/j.cclet.2022.05.056.

References

[1] T.M. Rawson, R.C. Wilson, A. Holmes, Clin. Microbiol. Infect. 27 (2021) 9–11.
[2] C. Liu, Y. Wen, W. Wan, J. Lei, X. Jiang, Int. Immunopharmacol. 90 (2021) 107157.
[3] S. Yu, G. Li, R. Liu, D. Ma, W. Xue, Adv. Funct. Mater. 28 (2018) 1707440.
[4] S. Yu, G. Li, P. Zhao, et al., Adv. Funct. Mater. 29 (2019) 1905697.
[5] S. Wu, Y. Huang, J. Yan, et al., Adv. Funct. Mater. 31 (2021) 2103442.
[6] E. Bakkeren, M. Diard, W.D. Hardt, Nat. Rev. Microbiol. 18 (2020) 479–490.
[7] D.G. Joakim Larsson, C.F. Flach, Nat. Rev. Microbiol. (20) (2022) 257–269.
[8] L. Jin, X. Liu, C. Bian, et al., Chin. Chem. Lett. 31 (2020) 2137–2141.
[9] H. Yan, H. Ni, Y. Yang, et al., Chin. Chem. Lett. 31 (2020) 1792–1796.
[10] T.M. Rawson, R.C. Wilson, D. O'Hare, et al., Nat. Rev. Microbiol. 19 (2021) 747–758.
[11] M. Miethke, M. Pieroni, T. Weber, et al., Nat. Rev. Chem. 5 (2021) 726–749.
[12] J. O'Neill, Tacking drug-resistant infections globally: Final report and recommendations, Review on Antimicrobial Resistance, Government of the United Kingdom, 2016, pp. 1–84.
[13] P.P. Kalelkar, M. Riddick, A.J. Garia, Nat. Rev. Mater. 7 (2022) 39–54.
[14] W. Li, E.S. Thian, M. Wang, Z. Wang, L. Ren, Adv. Sci. 8 (2021) 100368.
[15] Z. Vanic, M.W. Joraholmen, N. Skalko-Basnet, Adv. Drug Deliv. Rev. 178 (2021) 113855.
[16] J.M.V. Makabenta, A. Nabawy, C.H. Li, et al., Nat. Rev. Microbiol. 19 (2021) 23–36.
[17] F. Xiao, B. Cao, L. Wen, et al., Chin. Chem. Lett. 31 (2020) 2516–2519.
[18] Y. Li, W. Xiu, K. Yang, et al., Mater. Horiz. 8 (2021) 1264–1271.
[19] D. Li, T. Chen, Y. Zhang, Y. Xu, H. Niu, Adv. Healthcare Mater. 10 (2021) 2100716.
[20] M. Song, Y. Cheng, Y. Tian, et al., Adv. Funct. Mater. 30 (2020) 2003587.
[21] J. Huo, Q. Jia, H. Huang, et al., Chem. Soc. Rev. 50 (2021) 8762–8789.
[22] J.W. Xu, K. Yao, Z.K. Xu, Nanoscale 11 (2019) 8680–8691.
[23] C.R. McCollum, J.R. Bertram, P. Nagpal, A. Chatterjee, ACS Appl. Mater. Interfaces 13 (2021) 30404–30419.
[24] T.W. Chang, H. Ko, W.S. Huang, et al., Chem. Eng. J. 428 (2022) 131237.
[25] X. Guo, B. Cao, C. Wang, S. Lu, X. Hu, Nanoscale 12 (2020) 7651–7659.
[26] C. Cao, N. Yang, Y. Zhao, et al., Nano Today 39 (2021) 101165.
[27] Z. Tang, Y. Liu, M. He, W. Bu, Angew. Chem. Int. Ed. 58 (2019) 946–956.
[28] C. Wang, W. Zhao, B. Cao, et al., Chem. Mater. 32 (2020) 7725–7738.
[29] G. Guo, H. Zhang, H. Shen, et al., ACS Nano 14 (2020) 13391–13405.
[30] Q. Xu, Y. Hua, Y. Zhang, et al., Adv. Healthcare Mater. 10 (2021) 2101374.
[31] N. Yang, H. Guo, C. Cao, et al., Biomaterials 275 (2021) 120918.
[32] X. Zhu, X. Chen, Z. Jia, et al., J. Colloid Interface Sci. 603 (2021) 615–632.
[33] Y. Shi, J. Yin, Q. Peng, et al., Biomater. Sci. 8 (2020) 6093–6099.
[34] X. Lin, Y. Fang, Z. Hao, et al., Small 17 (2021) 2103303.
[35] E.A.D.R. Hans, M.D. Regulacio, Chem. Eur. J. 27 (2021) 11030–11040.

[36] A. Nain, S.C. Wei, Y.F. Lin, et al., ACS Appl. Mater. Interfaces 13 (2021) 7865–7878.
[37] Y. Zhou, Z. Chen, S. Zeng, et al., ACS Appl. Mater. Interfaces 13 (2021) 53659–53670.
[38] C. Dong, W. Feng, W. Xu, et al., Adv. Sci. 7 (2020) 2001549.
[39] X. Yu, T. Shang, G. Zheng, et al., Chin. Chem. Lett. 33 (2022) 1895–1900.
[40] Y. Yu, P. Li, C. Zhu, et al., Adv. Funct. Mater. 29 (2019) 1904402.
[41] Z. Ren, S. Sun, R. Sun, et al., Adv. Mater. 32 (2020) 1906024.
[42] Z. Guo, W. Xie, J. Lu, et al., J. Mater. Chem. B 9 (2021) 4098–4110.
[43] T. Liu, M. Zhang, W. Liu, et al., ACS Nano 12 (2018) 3917–3927.
[44] R. Shen, W. Chen, Q. Peng, et al., Chem 5 (2019) 2099–2110.
[45] X. Deng, K. Li, X. Cai, et al., Adv. Mater. 29 (2017) 1701266.